ACS APPLIED MATERIALS & INTERFACES

Research Article

www.acsami.org

Synthesis of POSS-Based Ionic Conductors with Low Glass Transition Temperatures for Efficient Solid-State Dye-Sensitized Solar Cells

Wei Zhang and Zhong-Sheng Wang*

Department of Chemistry, Lab of Advanced Materials, Collaborative Innovation Center of Chemistry for Energy Materials, Fudan University, 2205 Songhu Road, Shanghai 200438, P. R. China

Supporting Information

ABSTRACT: Replacing liquid-state electrolytes with solid-state electrolytes has been proven to be an effective way to improve the durability of dye-sensitized solar cells (DSSCs). We report herein the synthesis of amorphous ionic conductors based on polyhedral oligomeric silsesquioxane (POSS) with low glass transition temperatures for solid-state DSSCs. As the ionic conductor is amorphous and in the elastomeric state at the operating temperature of DSSCs, good pore filling in the TiO_2 film and good interfacial contact between the solid-state electrolyte and the TiO_2 film can be guaranteed. When the POSS-based ionic conductor containing an allyl group is doped with only iodine as the solid-state electrolyte without any other additives, power conversion efficiency of 6.29% has been achieved with good long-term stability under one-sun soaking for 1000 h.

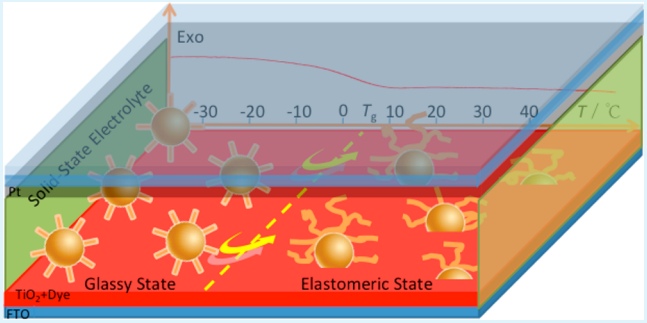

KEYWORDS: *dye-sensitized solar cells, POSS, solid-state electrolyte, ionic conductor, glass transition temperature*

1. INTRODUCTION

Tremendous attention on dye-sensitized solar cells (DSSCs) has led to huge developments in this field in the last two decades, since B. O'Regan and M. Grätzel published a seminal paper on DSSCs with fairly good photovoltaic performance.[1] Potential low cost, high power conversion efficiency, easy fabrication, and environmental friendliness are the main reasons for continuous input on DSSCs. A typical DSSC consists of a dye-sensitized nanocrystalline semiconductor electrode, a redox electrolyte and a counter electrode. The commonly used electrolyte for high-performance DSSCs is iodide/triiodide (I^-/I_3^-) dissolved in a volatile organic solvent, which has achieved a power conversion efficiency of higher than 11%.[2]

However, the leakage or volatilization of the liquid solvent in the electrolyte significantly deteriorates the long-term stability of DSSCs.[3,4] Considerable efforts have been made to replace the volatile organic solvents with ionic liquids,[5,6] but they are still a type of liquid material and leakage during long-term operation is difficult to avoid. Gel electrolytes[7] have also been reported as the quasi-solid-state electrolyte in DSSCs, but the volatilization of the solvent in the gel is inevitable. To make the DSSC device more stable, solid-state DSSCs (ssDSSCs) are desirable. P-type inorganic semiconductors (CuI, $CsSnI_{2.95}F_{0.05}$, etc.),[8,9] organic hole-transporting materials,[10,11] and ionic conductors based on imidazolium iodide[12,13] have been used to fabricate ssDSSCs. Among the solid-state electrolytes, ionic conductors based on imidazolium iodides are promising candidates for applications in ssDSSCs.[14] However, the problem of ionic conductors is the crystallization,[15] which leads to poor filling of pores in the TiO_2 film and hence hinders efficient dye regeneration.[16] To solve such a problem, we added crystal growth inhibitor to the electrolyte, which improved efficiency significantly.[15] To avoid crystallization of the ionic conductor, we designed and synthesized an amorphous ionic conductor[17] by linking the ionic liquid unit to polyhedral oligomeric silsesquioxane (POSS),[18] which could achieve good performance without addition of crystal growth inhibitor. However, the POSS-based ionic conductor we reported previously[17] is in the glassy state under the operating temperature of DSSCs due to its high glass transition temperature (52 °C), which is not favorable for good interfacial contact between the solid-state electrolyte and TiO_2 film. To improve interfacial wetting of solid-state electrolyte on the TiO_2 film, it is worth developing new ionic conductors with low glass transition temperatures for use in ssDSSCs.

Because of its unique three-dimensional cage structure composed of Si−O bonds, different functional groups can be easily attached to POSS to expand its properties.[19,20] Furthermore, the introduction of POSS that has a large free volume to the imidazolium iodide can endow the ionic conductor with the properties of polymers or oligomers. It is thus anticipated that POSS-based ionic conductors with low glass transition temperatures can be obtained by structural modifications. In this work, we synthesized two ionic

Received: April 29, 2014
Accepted: June 16, 2014
Published: June 16, 2014

Scheme 1. Synthetic Route for Ionic Conductors POSS-1 and POSS-2

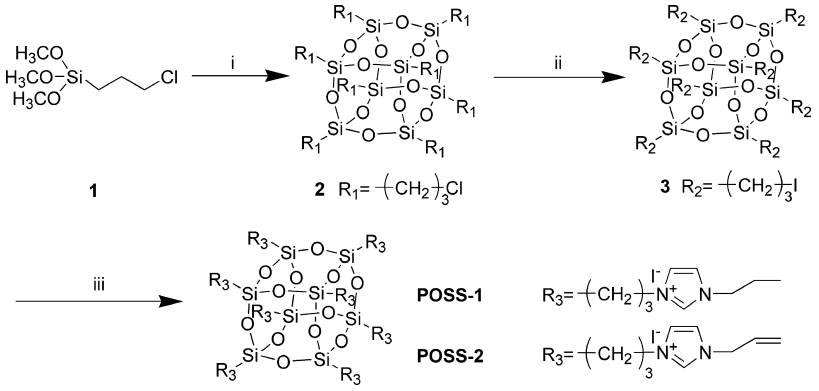

conductors by linking POSS to propyl and allyl substituted imidazolium iodides, and the glass transition temperatures are successfully lowered to be 5 and 6 °C, respectively. When binary solid-state electrolyte prepared by blending the ionic conductor and appropriate amount of iodine without any other additives is used to operate the ssDSSCs, good power conversion efficiency has been achieved using an organic dye[21] (see Figure S1 in the Supporting Information) as the sensitizer.

2. EXPERIMENTAL SECTION

2.1. Materials and Reagents. Iodine (I_2), sodium iodide (NaI), 3-chloropropyltrimethoxysilane, tetrabutylammonium iodide and iodopropane were purchased from Aladdin. Organic solvents used in this work were purified using standard processes. Other chemical reagents were used as received from commercial sources without further purification. Transparent conductive glass (F-doped SnO_2, FTO, 14 Ω, transmittance of 90%, Nippon Sheet Glass Co., Japan) was used as the substrate for the fabrication of TiO_2 thin film electrodes.

2.2. Synthesis of Ionic Conductors. The synthetic route for ionic conductors (**POSS-1** and **POSS-2**) is shown in Scheme 1, and the synthetic details are described below:

2.2.1. Synthesis of Compound ***2****.* Compound **2** was synthesized according to the method described by Dittmar et al.[22] After mixing 3-chloropropyltrimethoxysilane (3.975 g, 0.02 mol) and concentrated hydrochloric acid (4.5 mL) in methanol (90 mL), the hydrolysis and the rearrangement reactions were allowed to carry out for 3 days at 60 °C, and then colorless crystals were obtained after drying in vacuum with a yield of 20%. ^{1}H NMR ($CDCl_3$, 400 MHz, δ ppm): 3.54 (t, 16H); 1.87 (m, 16H); 0.80 (t, 16H). ^{13}C NMR ($CDCl_3$, 100 MHz, δ ppm): 47.3, 26.5, 9.5.

2.2.2. Synthesis of compound ***3****.* A mixture of **2** (2.0 g, 2 mmol), sodium iodide (9.0 g, 60 mmol), tetrabutylammonium iodide (22.0 g, 60 mmol) and iodopropane (10.0 mL, 8 mmol) in 2-butanone (160 mL) was heated to reflux for 72 h.[23] After the reaction system was cooled to RT, the solvent was evaporated and the residue was dissolved in water (100 mL) and extracted with CH_2Cl_2 (100 mL). The organic phase was washed twice with water and once with brine (100 mL each) followed by drying over Na_2SO_4. The solvent was evaporated and the residue was rinsed with CH_3OH and filtered. The filter cake was washed several times with CH_3OH and dried in a vacuum to yield 2.96 g (86.5%) of **3** as a colorless solid. ^{1}H NMR ($CDCl_3$, 400 MHz, δ ppm): 3.22 (t, 16H); 1.92 (m, 16H); 0.78 (t, 16H). ^{13}C NMR ($CDCl_3$, 100 MHz, δ ppm): 27.6, 13.7, 10.4.

2.2.3. Synthesis of Compound ***POSS-1****.* 1.3 equiv. of 1-propylimidazolium (1.43 g, 13 mmol) and **3** (2.21 g, 1.25 mmol) were dissolved in THF (20 mL) and the mixture was stirred at RT for 48 h. Pale and viscous solid was obtained after pouring off the upper solution. Washing the solid with THF followed by drying for three cycles yields a pale solid (2.71 g) of **POSS-1** in a yield of 82%. ^{1}H NMR (DMSO-d_6, 400 MHz, δ ppm): 9.36 (d, 8H); 7.90 (d, 8H); 7.86 (s, 8H); 4.20 (t, 16H); 4.16 (t, 16H); 1.82 (m, 16H); 1.80 (m, 16H); 0.82 (t, 24H); 0.58 (t, 16H). ^{13}C NMR (DMSO-d_6, 100 MHz, δ ppm): 136.7, 122.9, 67.7, 51.5, 51.0, 25.8, 23.9, 11.2, 8.6. ^{29}Si NMR (DMSO-d_6, 100 MHz, δ ppm): −66.89.

2.2.4. Synthesis of Compound ***POSS-2****.* 1.3 equiv. of 1-allylimidazolium (1.40 g, 13 mmol) and **3** (2.21 g, 1.25 mmol) were dissolved in THF (20 mL) and the mixture was stirred at RT for 48 h. Pale and viscous solid was obtained after pouring off the upper solution. After washing the solid with THF followed by drying for three cycles, a pale solid (2.63 g) of **POSS-2** in a yield of 80% was obtained. ^{1}H NMR (DMSO-d_6, 400 MHz, δ ppm): 9.32 (d, 8H); 7.92 (d, 8H); 7.78 (s, 8H); 6.06 (m, 8H); 5.33 (m, 16H); 4.88 (m, 16H); 4.21 (t, 16H); 1.80 (t, 16H); 0.57 (t, 16H). ^{13}C NMR (DMSO-d_6, 100 MHz, δ ppm): 136.8, 132.3, 123.0, 121.1, 67.7, 51.6, 25.8, 24.0, 8.6. ^{29}Si NMR (DMSO-d_6, 100 MHz, δ ppm): −66.88.

2.3. Fabrication of DSSCs. TiO_2 films (12 μm) composed of 6 μm nanoparticle (20 nm) layer in direct contact with the FTO substrate and 6 μm light scattering particle (80% 20 nm TiO_2+20% 100 nm TiO_2) layer were fabricated with a screen printing method[24] and used in this study. The films were sintered at 500 °C for 2 h to achieve good necking of neighboring TiO_2 particles. The film thickness was measured with a surface profiler (Veeco Dektak 150, USA). The sintered films were then treated with 0.05 M $TiCl_4$ aqueous solution at 70 °C for 30 min followed by calcinations at 450 °C for 30 min. When TiO_2 electrodes were cooled down to 120 °C, the electrodes were dipped in dye solutions (see Figure S1 in the Supporting Information, 0.3 mM in toluene) for 24 h at RT. The Pt-coated FTO as the counter electrode and the dye-loaded film as the working electrode were separated by a hot-melt Surlyn film (30 μm) and sealed together by pressing them under heat. The methanol solution of the solid electrolyte was injected repeatedly into the interspace between the working and counter electrodes from the two holes predrilled on the back of the counter electrode and dried on a hot plate with the temperature of 50 °C until the TiO_2 porous film was filled with solid-state electrolyte. The cell was further dried at 50 °C under vacuum for 1 h to remove methanol. Finally, the two holes were sealed with a Surlyn film covered with a thin glass slide under heat.

2.4. Characterizations and Photovoltaic Measurements. ^{1}H NMR and ^{13}C NMR spectra were recorded on a Varian 400 MHz NMR spectrometer with tetramethylsilane (TMS) as an internal standard. ^{29}Si NMR spectra were recorded on a DMX-500 instrument with tetramethylsilane (TMS) as an internal standard. High-resolution mass spectroscopy (HRMS) was performed using a Waters LCT Premier XE spectrometer. Fourier transform infrared (FT-IR) measurements were performed on Shimadzu IRAffinity-1 FT-IR spectrometer. Thermogravimetric (TG) analysis was performed on a TG-DTA 2000S system (Mac Sciences Co. Ltd., Yokohama, Japan) at a heating rate of 10 °C min^{-1}. Differential scanning calorimetry (DSC) was studied on a Shimadzu DSC-60A at a heating rate of 5 °C min^{-1}. X-ray diffraction (XRD) patterns for the ionic conductors were measured on an X-ray powder diffractometer (D8 Advance, Bruker,

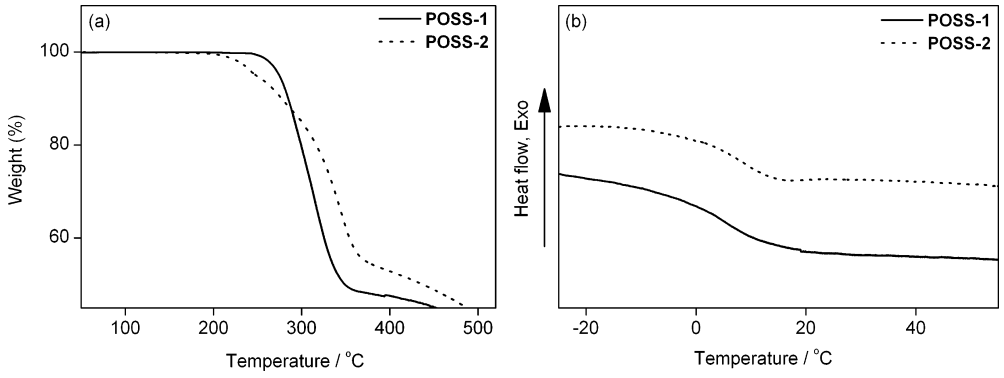

Figure 1. (a) TG and (b) DSC curves of **POSS-1** and **POSS-2**.

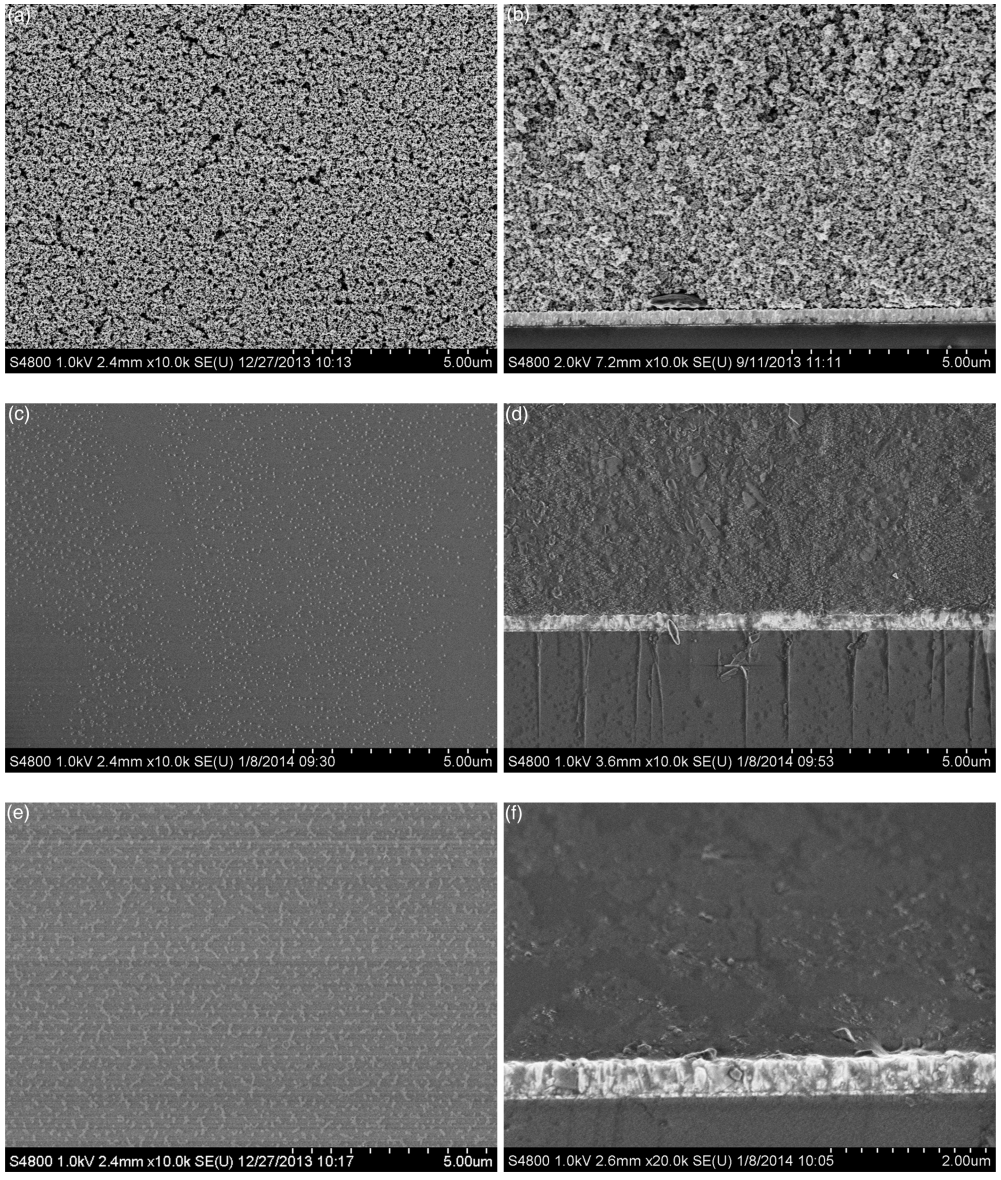

Figure 2. (a, c, e) Top and (b, d, f) side view SEM images of (a, b) the bare TiO_2 film, (c, d) the TiO_2 film filled with **POSS-1**/I_2, and (e, f) the TiO_2 film filled with **POSS-2**/I_2 followed by drying.

Germany) with Cu Kα radiation (λ = 0.154 nm). The morphology of the TiO_2 films before and after solid-state electrolyte addition was examined with a field-emitting scanning electron microscope (FESEM, S-4800, Hitachi, Japan). The ionic conductivity of the solid electrolytes, which were sandwiched in sealed dummy cells made up of two identical Pt electrodes separated with a Surlyn film (30 μm), was determined with an ac impedance technique (frequency range: 10 mHz to 100 kHz) using an electrochemical workstation (Zahner

CIMPS-1, Germany). The applied bias and ac amplitude were set at 0 V and 10 mV, respectively. The working performance of the DSSC was tested by recording the current density−voltage (J−V) curves with a Keithley 2400 source meter (Oriel) under illumination of simulated AM1.5G solar light coming from a solar simulator (Oriel-94043A equipped with a Xe lamp and an AM1.5G filter). The light intensity was calibrated using a standard Si solar cell (Newport 91150). Action spectra of the incident monochromatic photon-to-electron conversion efficiency (IPCE) for the solar cells were obtained with an Oriel-74125 system (Oriel Instruments). The intensity of monochromatic light was measured with a Si detector (Oriel-71640). The electron lifetimes were measured with controlled intensity modulated photovoltage spectroscopy (IMVS). IMVS was carried out on an electrochemical workstation (Zahner XPOT), which includes a green light-emitting diode (LED, 532 nm) and the corresponding control system.

3. RESULTS AND DISCUSSION

3.1. Characterizations of POSS-1 and POSS-2. Figure S2 in the Supporting Information shows the FT-IR spectra for **POSS-1** and **POSS-2**. The IR band of Si−O in silsesquioxane cage appears at 1118 cm^{-1}, which is in consistence with the reference.[25] The bands at 1626 and 1561 cm^{-1} are assigned to the C═C and C═N stretching in the imidazolium ring, respectively, while the bands at 3136 and 3078 cm^{-1} are attributed to C−H stretching in the imidazolium ring.[26] The main difference of IR spectra between **POSS-1** and **POSS-2** is the band at 1644 cm^{-1}, which appears for **POSS-2** because of the presence of allyl group but is absent for **POSS-1**. Figure S3 in the Supporting Information shows HRMS for the two POSS-based ionic conductors. The peak at m/z 1197.6 is attributed to the cation ($Si_8O_{12}C_{72}N_{16}I_6H_{128}^{2+}$) in **POSS-1**, while the peak at m/z 1189.6 is attributed to the cation ($Si_8O_{12}C_{72}N_{16}I_6H_{112}^{2+}$) in **POSS-2.**

Figure 1a shows the TG curves for **POSS-1** and **POSS-2**. The starting decomposition temperatures, at which the decomposition begins, have been determined by TG analysis. **POSS-1** and **POSS-2** start to decompose at 242 and 203 °C, respectively. The ionic conductor containing the ally group shows lower decomposition onset than its corresponding propyl counterpart, likely due to the rigidity of the carbon−carbon double bond. The TG results indicate that both ionic conductors have very good thermal stability below 200 °C, making them good candidates for outdoor applications of solar cells. Figure 1b displays DSC curves of **POSS-1** and **POSS-2**. Typical glass transition process is observed for both ionic conductors due to the presence of POSS unit. **POSS-1** displays a T_g of 5 °C, whereas **POSS-2** displays a T_g of 6 °C. As propyl is more flexible than allyl, it is reasonable that the T_g for **POSS-1** is lower than that for **POSS-2**. When such ionic conductors are used as solid-state electrolytes of ssDSSCs during device operation in the temperature higher than the glass transition temperature but lower than the decomposition temperature, they are in the elastomeric state. As we know, molecules can twist and stretch easily in elastomeric state,[27] which is favorable for efficient ssDSSCs.[28]

Generally, glass transition process can be the proof that the obtained ionic conductors are amorphous. To further characterize the amorphous feature, powder X-ray diffraction is performed. Figure S4 in the Supporting Information shows XRD patterns of **POSS-1** and **POSS-2**. Only one broad peak is observed for both ionic conductors, indicating that **POSS-1** and **POSS-2** are amorphous. This is advantageous to pore filling of TiO_2 as compared with some easy-crystallized ionic conductors to be used as solid-state electrolytes.[15] Figure 2 displays top and side views of SEM images of TiO_2 films before and after filling of solid **POSS-1**/I_2 and **POSS-2**/I_2 electrolytes, respectively. Pores among TiO_2 particles were clearly observed from both top and side SEM views for the bare TiO_2 film. However, when either **POSS-1**/I_2 or **POSS-2**/I_2 was added into the TiO_2 film, the TiO_2 surface became smooth and the pores were invisible, indicating that both **POSS-1**/I_2 and **POSS-2**/I_2 filled the TiO_2 pores sufficiently. By contrast, the crystallized ionic conductors tended to form large crystals during electrolyte injection and could not fill the pores well as we reported previously.[15]

3.2. Ionic Conductivity. The ionic conductivity was measured with the electrochemical impedance on dummy cells constructed with two identical platinized FTO glass substrates and filled with the solid electrolyte. The as-synthesized **POSS-1** exhibits higher conductivity (0.042 mS cm^{-1}) than the as-synthesized **POSS-2** (0.022 mS cm^{-1}). For the as-synthesized ionic conductors, the ionic conductivity depends on the physical diffusion[13] of ions. As propyl is more flexible than allyl, it is reasonable that the ionic diffusion in **POSS-1** is faster than that in **POSS-2**, and therefore the former shows higher conductivity than the latter.

When appropriate amount of iodine is added to the ionic conductor (molar ratio of POSS:I_2 = 1.5/1, the same below), the conductivity is significantly improved to 0.46 and 1.16 mS cm^{-1} for **POSS-1**/I_2 and **POSS-2**/I_2, respectively. The significant increase in conductivity is attributed to efficient Grotthus charge exchange.[29] As reported by Thorsmølle et al.,[30] the Grotthus mechanism can contribute to ionic charge transport in 1-methyl-3-propylimidazolium iodide at high iodine concentration. The main reason is that high iodine/iodide packing density can reduce the distance between iodide/polyiodide species, which enhances Grotthus bond exchange ($I^- + I_3^- = I_3^- + I^-$) and thus leads to extraordinarily efficient charge transport.[30] Therefore, for the ionic conductor mixed with iodine, the ionic conductivity depends on Grotthus charge exchange.[31] Although the as-synthesized **POSS-1** exhibits higher conductivity than the as-synthesized **POSS-2**, the latter shows higher conductivity when iodine is mixed with the ionic conductor. This indicates that the Grotthus charge exchange rate in the **POSS-2**/I_2 mixture is faster than that in the **POSS-1**/I_2 mixture, which dominates the ionic conductivity upon iodine doping. The Grotthus charge exchange rate is affected by intermolecular π−π interactions when the added amount of iodine is controlled the same. Owing to the presence of allyl groups, the π−π interactions for **POSS-2** are stronger than that for **POSS-1**, which is favorable for efficient Grotthus charge exchange and hence higher conductivity.[32]

The temperature dependence of conductivity for the ionic conductors mixed with iodine is shown in Figure 3. It can be seen from Figure 3 that conductivity increases with temperature and can be fitted well by the Arrhenius equation[33]

$$\sigma = \sigma_o \exp(-E_a/kT) \quad (1)$$

where σ_o is a constant, E_a is the activation energy, k is Boltzmann's constant, and T is the absolute temperature. The linear dependence of $\ln\sigma$ on $1/T$ indicates that the conductivity of the solid electrolyte is attributed to ionic conduction, which originates from the charge transfer along the polyiodide chain according to the relay-type Grotthus mechanism. Charge transfer along the polyiodide chain just looks like movements of iodide and triiodide in opposite directions.

3.3. Photovoltaic Performance. The current−voltage characteristics of DSSCs were tested under simulated

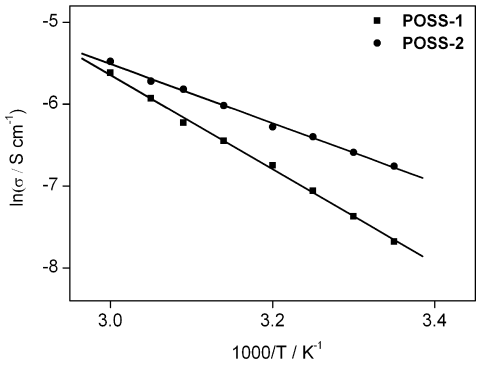

Figure 3. Temperature dependence of ionic conductivity for **POSS-1**/I_2 and **POSS-2**/I_2 (molar ratio 1.5/1).

AM1.5G illumination (100 mW cm^{-2}). Figure 4a illustrates the $J-V$ curves of cells with the solid-state electrolytes of **POSS-1**/I_2 (molar ratio of 1.5/1) and **POSS-2**/I_2 (molar ratio of 1.5/1), respectively. The **POSS-1**/I_2 based ssDSSC produced a short-circuit photocurrent (J_{sc}) of 10.93 mA cm^{-2}, an open-circuit photovoltage (V_{oc}) of 0.71 V, and a fill factor (FF) of 0.68, corresponding to a power conversion efficiency (η) of 5.28%. Under the same condition, the ssDSSC-based on **POSS-2**/I_2 generated a J_{sc} of 12.15 mA cm^{-2}, a V_{oc} of 0.74 V, and an FF of 0.70, corresponding to a η of 6.29%. The higher J_{sc} and FF for the ssDSSC with **POSS-2**/I_2 is mainly attributed to its higher conductivity, as compared to the ssDSSC with **POSS-1**/I_2. To highlight the advantage of low glass-transition temperature, we did a control experiment using the previously reported POSS-based ionic conductor[17] with a higher T_g (52 °C). The ssDSSC with the previously reported POSS-based ionic conductor[17] produced efficiency of 4.40% (J_{sc} = 9.96 mA cm^{-2}, V_{oc} = 0.64 V, FF = 0.69) under the same conditions and the same iodine amount, which was much lower than the efficiency obtained from the ionic conductor with lower T_g. As lower T_g can make the solid electrolyte in the elastomeric state under the device operating temperature, which is favorable for good interfacial contact between electrolyte and the dye-loaded TiO_2 film and hence efficient dye regeneration, it is reasonable that the ionic conductor with a lower T_g can regenerate dye cation efficiently and thus achieve higher current and better photovoltaic performance.

The photovoltaic performance can be enhanced by using a better dye having broad absorption and high extinction coefficient. In addition, the performance is also influenced by the structure of photoanode. Recently, Kuang et al. reported interesting hyperbranched anatase titania architectures,[34] branched nanowire-coated macroporous metal oxide electrodes,[35] and ultralong anatase titania nanowire arrays with multilayered configuration.[36] These novel structures are suitable for solid-state DSSCs considering the favorable attributes, such as high surface area, strong light scattering and fast electron transport properties. It is expected to achieve higher efficiency when our electrolytes are combined with these interesting photoanodes.

Figure 4b shows the IPCE spectra for the two ssDSSCs. The IPCE values for **POSS-2**/I_2 are higher than those for **POSS-1**/I_2 in the spectral range of 350−650 nm, accounting for the J_{sc} difference. The difference of IPCE for the two ionic conductors is also attributed to the different ionic conductivity.

Figure 5a shows the dependence of J_{sc} on light intensity. For **POSS-1**/I_2-based device, J_{sc} increased linearly with light intensity in the range of 10−80 mW cm^{-2} and then increased more slowly with further increasing light intensity up to 100 mW cm^{-2}. This means that the ionic conductivity of **POSS-1**/I_2 is high enough for photocurrent generation at light intensity below 80 mW cm^{-2} but not sufficiently high for photocurrent generation at full-sun irradiation. However, J_{sc} increased linearly with light intensity in the range of 10−100 mW cm^{-2} for **POSS**-2/I_2-based device, indicating that the ionic movements in **POSS-2**/I_2 caused by the Grotthus charge exchange did not limit the photocurrent generation up to 100 mW cm^{-2}. As compared to **POSS-1**/I_2 based cell, the **POSS-2**/I_2-based cell showed a linear dependence of J_{sc} on light intensity in a wider range because of its higher conductivity.

The dependence of V_{oc} on light intensity is shown in Figure 5b. For **POSS-1**/I_2-based device, V_{oc} increased linearly with the logarithm of light intensity in the range of 10−80 mW cm^{-2} and then increased more slowly with further increasing light intensity up to 100 mW cm^{-2}. For **POSS-2**/I_2 based device, V_{oc} increased linearly with the logarithm of light intensity in the range of 10−100 mW cm^{-2}. V_{oc} is defined as the difference between the quasi-Fermi level of dye-loaded TiO_2 under light and the redox potential of the redox electrolyte. V_{oc} is mainly due to the light-induced change of electron density in the conduction band of TiO_2 and usually increases linearly with the logarithm of J_{sc}.[37] Therefore, it is reasonable to observe a linear dependence of V_{oc} on the logarithm of light intensity in the range where J_{sc} increases linearly with light intensity.

The influence of temperature on solar cell performance was also investigated in the temperature range of 25−80 °C, and the

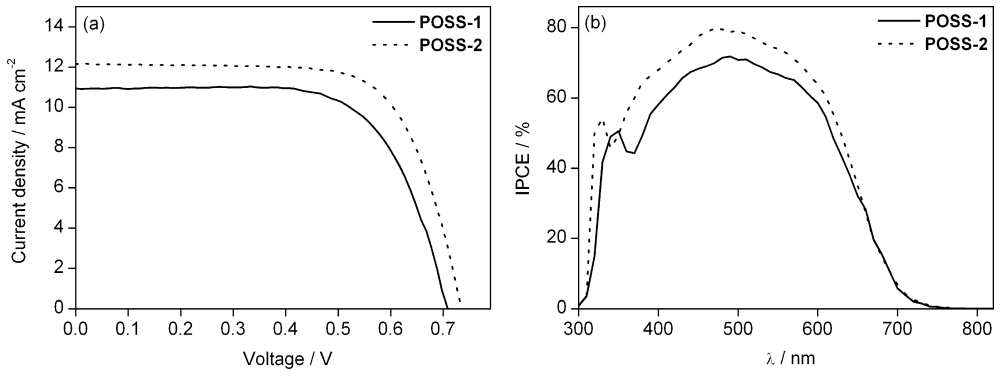

Figure 4. (a) $J-V$ curves and (b) IPCE spectra for ssDSSCs based on **POSS-1**/I_2 and **POSS-2**/I_2, respectively. Four parallel DSSCs for each sample were measured with standard deviation errors of less than 0.2% and 2% in absolute power conversion efficiency and IPCE, respectively.

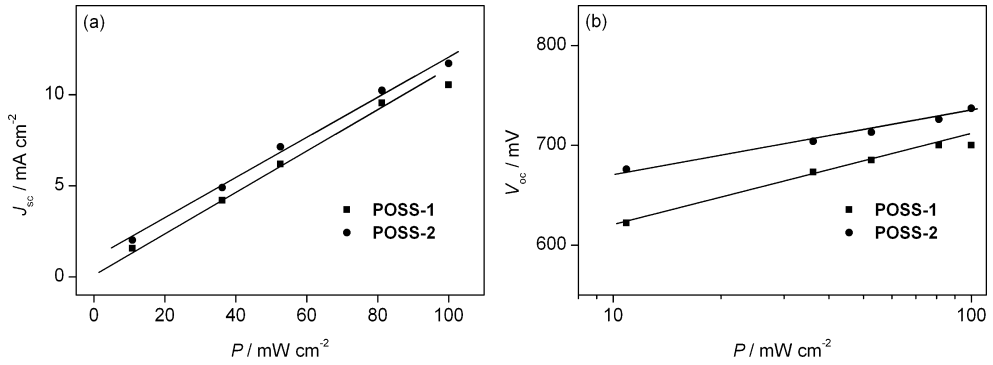

Figure 5. Light intensity dependence of (a) J_{sc} and (b) V_{oc}.

photovoltaic data are summarized in Table 1. For both electrolytes, J_{sc} increased gradually with temperature because

Table 1. Influence of Temperature on Solar Cell Performance

	T (°C)	J_{sc}/mA cm^{-2}	V_{oc}/mV	FF	η (%)
POSS-1	25	10.70	713	0.68	5.19
	40	11.60	709	0.67	5.51
	60	12.39	699	0.67	5.80
	80	13.46	684	0.65	5.98
POSS-2	25	11.58	743	0.71	6.11
	40	12.57	732	0.69	6.35
	60	12.91	724	0.68	6.36
	80	13.37	703	0.68	6.39

of the increased conductivity (Figure 3), whereas V_{oc} decreased gradually because of the possible positive shift of conduction band edge of TiO_2 with temperature.[38] J_{sc} was similar at 80 °C for both electrolytes due to their similar conductivity at high temperature (Figure 3). The power conversion efficiency increased gradually with temperature for **POSS-1** while it increased from 25 to 40 °C for **POSS-2** followed by a negligible change with further increasing temperature. The difference of power conversion efficiency between the two electrolytes became smaller with temperature because of the reduced difference of conductivity with temperature (Figure 3).

The increase in V_{oc} by 0.03 V from **POSS-1**/I_2 to **POSS-2**/I_2 can be explained by the different charge recombination rate. Figure 6 shows the electron lifetime against charge density for

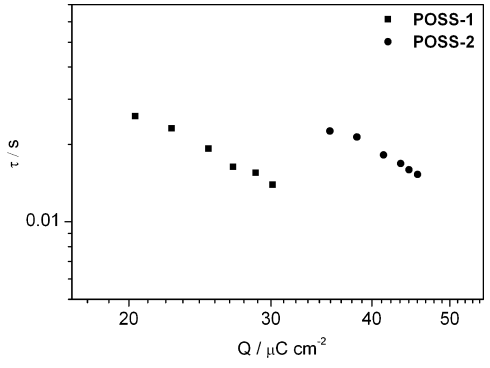

Figure 6. Electron lifetime against charge density for **POSS-1**/I_2- and **POSS-2**/I_2-based ssDSSCs. Four parallel DSSCs for each sample were measured with relative standard deviation errors of less than 10% in electron lifetime.

POSS-1/I_2 and **POSS-2**/I_2 based ssDSSCs. At the same charge density, the electron lifetime of **POSS-2**/I_2 based ssDSSC is about 2.5 times that of **POSS-1**/I_2 based ssDSSC. This suggests that charge recombination between electrons in TiO_2 film and I_3^- for **POSS-2**/I_2 is significantly retarded by the stronger $\pi-\pi$ stacking interactions between the allyl groups and imidazolium rings, as compared with **POSS-1**/I_2, which is responsible for the higher V_{oc}.

Long-term stability is one of the critical parameters for practical applications. The performance of the ssDSSC was recorded over a period of 1000 h under one-sun soaking at RT using an unoptimizable cell with **POSS-2**/I_2 (Figure 7). The

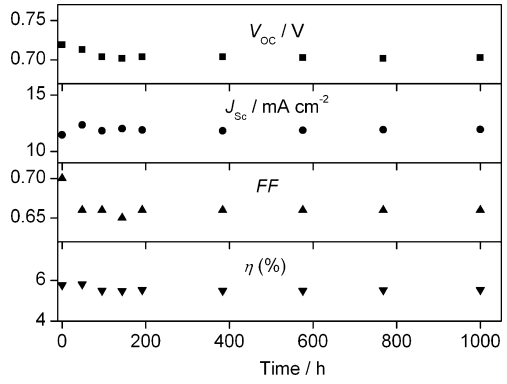

Figure 7. Performance evolution of the ssDSSC based on **POSS-2**/I_2 under one-sun soaking for 1000 h.

initial η was 5.77% (J_{sc} = 11.46 mA cm^{-2}, V_{oc} = 719 mV, FF = 0.70). At the beginning stage up to 100 h, J_{sc} increased while V_{oc} and FF decreased, respectively. Afterward, all the photovoltaic parameters hardly changed up to 1000 h of light soaking likely due to the aging of the device. Compared to the initial performance, J_{sc} increased by 4%, V_{oc} decreased by 2%, FF decreased by 6%, and η decreased by 4%. These data suggest that the ssDSSC with this solid-state electrolyte is long-term stable. The amorphous feature of the POSS-based solid electrolyte with low glass transition temperature is advantageous to forming good interfacial contacts between solid electrolyte and electrodes. This is the main reason that the solid device remains stable during light soaking.

4. CONCLUSIONS

In summary, novel amorphous ionic conductors with low glass transition temperatures have been designed and synthesized for use in ssDSSCs. As a result, good interfacial contact between

solid electrolytes and TiO_2 particles has been achieved due to the amorphous feature and low glass transition temperature. As compared to **POSS-1**, stronger intermolecular $\pi-\pi$ stacking interactions between the allyl groups and imidazolium rings can result in higher conductivity of **POSS-2**/I_2 and slower charge recombination. As a consequence, the ssDSSC based on **POSS-2**/I_2 exhibits better photovoltaic performance than that based on **POSS-1**/I_2. These findings favor the design of new ionic conductors for efficient ssDSSCs.

■ ASSOCIATED CONTENT

Ⓢ Supporting Information

The structure of the organic dyes used in this work; FTIR, HRMS, and XRD of the ionic conductors. This material is available free of charge via the Internet at http://pubs.acs.org.

■ AUTHOR INFORMATION

Corresponding Author

*E-mail: zs.wang@fudan.edu.cn. Tel/Fax: (+86)21-5163-0345.

Author Contributions

The manuscript was written through contributions of all authors. All authors have given approval to the final version of the manuscript.

Notes

The authors declare no competing financial interest.

■ ACKNOWLEDGMENTS

This work was financially supported by National Basic Research Program (2011CB933302) of China, STCSM (12JC1401500) and Jiangsu Major Program (BY2010147).

■ REFERENCES

(1) O'Regan, B.; Grätzel, M. A Low-Cost, High-Efficiency Solar Cell Based on Dye-Sensitized Colloidal TiO_2 Films. *Nature* **1991**, *353*, 737−740.

(2) Yu, Q.; Wang, Y.; Yi, Z.; Zu, N.; Zhang, J.; Zhang, M.; Wang, P. High-Efficiency Dye-Sensitized Solar Cells: The Influence of Lithium Ions on Exciton Dissociation, Charge Recombination, and Surface States. *ACS Nano* **2010**, *4*, 6032−6038.

(3) Li, D. M.; Li, H.; Luo, Y. H.; Li, K.; Meng, Q. B.; Armand, M.; Chen, L. Non-Corrosive, Non-Absorbing Organic Redox Couple for Dye-Sensitized Solar Cells. *Adv. Funct. Mater.* **2010**, *20*, 3358−3365.

(4) Li, D. M.; Qin, D.; Deng, M. H.; Luo, Y. H.; Meng, Q. B. Optimization The Solid-State Electrolytes for Dye-Sensitized Solar Cells. *Energy Environ. Sci.* **2009**, *2*, 283−291.

(5) Kuang, D. B.; Wang, P.; Ito, S.; Zakeeruddin, S. M.; Grätzel, M. Stable Mesoscopic Dye-Sensitized Solar Cells Based on Tetracyanoborate Ionic Liquid Electrolyte. *J. Am. Chem. Soc.* **2006**, *128*, 7732−7733.

(6) Bai, Y.; Cao, Y.; Zhang, J.; Wang, M.; Li, R.; Wang, P.; Zakeeruddin, S. M.; Grätzel, M. High-Performance Dye-Sensitized Solar Cells Based on Solvent-Free Electrolytes Produced from Eutectic Melts. *Nat. Mater.* **2008**, *7*, 626−630.

(7) Wang, P.; Zakeeruddin, S. M.; Moser, J. E.; Nazeeruddin, M. K.; Sekiguchi, T.; Grätzel, M. A Stable Quasi-Solid-State Dye-Sensitized Solar Cell with an Amphiphilic Ruthenium Sensitizer and Polymer Gel Electrolyte. *Nat. Mater.* **2003**, *7*, 402−407.

(8) Meng, Q.-B.; Takahashi, K.; Zhang, X.-T.; Sutanto, I.; Rao, T. N.; Sato, O.; Fujishima, A. Fabrication of An Efficient Solid-State Dye-Sensitized Solar Cell. *Langmuir* **2003**, *19*, 3572−3579.

(9) Chung, I.; Lee, B.; He, J.; Chang, R. P. H.; Kanatzidis, M. G. All-Solid-State Dye-Sensitized Solar Cells with High Efficiency. *Nature* **2012**, *485*, 486−489.

(10) Koh, J. K.; Kim, J.; Kim, B.; Kim, J. H.; Kim, E. Highly Efficient, Iodine-Free Dye-Sensitized Solar Cells with Solid-State Synthesis of Conducting Polymers. *Adv. Mater.* **2011**, *23*, 1641−1646.

(11) Cai, N.; Moon, S.-J.; Cevey-Ha, L.; Moehl, T.; Humphry-Baker, R.; Wang, P.; Zakeeruddin, S. M.; Grätzel, M. An Organic D-π-A Dye for Record Efficiency Solid-State Sensitized Heterojunction Solar Cells. *Nano Lett.* **2011**, *11*, 1452−1456.

(12) Wu, J. H.; Hao, S. C.; Lan, Z.; Lin, J. M.; Huang, M. L.; Huang, Y. F.; Li, P. J.; Yin, S.; Sato, T. An All-Solid-State Dye-Sensitized Solar Cell-Based Poly(N-alkyl-4-vinyl-pyridine iodide) Electrolyte with Efficiency of 5.64%. *J. Am. Chem. Soc.* **2008**, *130*, 11568−11569.

(13) Yamanaka, N.; Kawano, R.; Kubo, W.; Masaki, N.; Kitamura, T.; Wada, Y.; Watanabe, M.; Yanagida, S. Dye-Sensitized TiO_2 Solar Cells Using Imidazolium-Type Ionic Liquid Crystal Systems as Effective Electrolytes. *J. Phys. Chem. B* **2007**, *111*, 4763−4769.

(14) Wang, H.; Li, J.; Gong, F.; Zhou, G.; Wang, Z.-S. Ionic Conductor with High Conductivity as Single-Component Electrolyte for Efficient Solid-State Dye-Sensitized Solar Cells. *J. Am. Chem. Soc.* **2013**, *135*, 12627−12633.

(15) Wang, H.; Zhang, X.; Gong, F.; Zhou, G.; Wang, Z.-S. Novel Ester-Functionalized Solid-State Electrolyte for Highly Efficient All-Solid-State Dye-Sensitized Solar Cells. *Adv. Mater.* **2012**, *24*, 121−124.

(16) Kumara, G. R. R. A.; Konno, A.; Senadeera, G. K. R.; Jayaweera, P. V. V; Silva, D. B. R. A. D.; Tennakone, K. Dye-Sensitized Solar Cell with The Hole Collector p-CuSCN Deposited from A Solution in n-propyl Sulphide. *Sol. Energy Mater. Sol. Cells* **2001**, *69*, 195−199.

(17) Zhang, W.; Li, J.; Jiang, S. H.; Wang, Z.-S. POSS with Eight Imidazolium Iodide Arms for Efficient Solid-State Dye-Sensitized Solar Cells. *Chem. Commun.* **2014**, *50*, 1685−1687.

(18) Scott, D. W. Thermal Rearrangement of Branched-Chain Methylpolysiloxanes. *J. Am. Chem. Soc.* **1946**, *68*, 356−358.

(19) Chinnam, P. R.; Wunder, S. L. Self-Assembled Janus-Like Multi-Ionic Lithium Salts Form Nano-Structured Solid Polymer Electrolytes with High Ionic Conductivity and Li^+ Ion Transference Number. *J. Mater. Chem. A* **2013**, *1*, 1731−1739.

(20) Naka, K.; Shinke, R.; Yamada, M.; Belkada, F. D.; Aijo, Y.; Irie, Y.; Shankar, S. R.; Smaran, K. S.; Matsumi, N.; Tomita, S.; Sakurai, S. Synthesis of Imidazolium Salt-Terminated Poly(amidoamine)-Typed POSS-Core Dendrimers and Their Solution and Bulk Properties. *Polym. J.* **2014**, *46*, 42−51.

(21) Li, Y.; Wang, H.; Feng, Q. Y.; Zhou, G.; Wang, Z.-S. Gold Nanoparticles Inlaid TiO_2 Photoanodes: A Superior Candidate for High-Efficiency Dye-Sensitized Solar Cells. *Energy Environ. Sci.* **2013**, *6*, 2156−2165.

(22) Dittmar, U.; Hendan, J. B.; Floerke, U.; Marsmann, H. C. Funktionalisierte Octa-(Propylsilsesquioxane) $(3\text{-}XC_3H_6)_8(Si_8O_{12})$ Modellverbindungen Für oberflächenmodifizierte Kieselgele. *J. Organomet. Chem.* **1995**, *489*, 185−194.

(23) Heyl, D.; Rikowski, E.; Hoffmann, R. C.; Schneider, J. J.; Fessner, W. D. A "Clickable" Hybrid Nanocluster of Cubic Symmetry. *Chem.—Eur. J.* **2010**, *16*, 5544−5548.

(24) Wang, Z.-S.; Kawauchi, H.; Kashima, T.; Arakawa, H. Significant Influence of TiO_2 Photoelectrode Morphology on the Energy Conversion Efficiency of N719 Dye-Sensitized Solar Cell. *Coord. Chem. Rev.* **2004**, *248*, 1381−1389.

(25) Jerman, I.; Kozelj, M.; Orel, B. The Effect of Polyhedral Oligomeric Silsesquioxane Dispersant and Low Surface Energy Additives on Spectrally Selective Paint Coatings with Self-Cleaning Properties. *Sol. Energy Mater. Sol. Cells* **2010**, *94*, 232−245.

(26) Jerman, I.; Jovanovski, V.; Šurca Vuk, A.; Hočevar, S. B.; Gaberšček, M.; Jesih, A.; Orel, B. Ionic Conductivity, Infrared and Raman Spectroscopic Studies of 1-methyl-3-propylimidazolium Iodide Ionic Liquid with Added Iodine. *Electrochim. Acta* **2008**, *53*, 2281−2288.

(27) Lötters, J. C.; Olthuis, W.; Veltink, P. H.; Bergveld, P. The Mechanical Properties of The Rubber Elastic Polymer Polydimethylsiloxane for Sensor Applications. *J. Micromech. Microeng.* **1997**, *7*, 145−147.

(28) Wang, G.; Wang, L.; Zhuo, S.; Fang, S.; Lin, Y. An Iodine-Free Electrolyte Based on Ionic Liquid Polymers for All-Solid-State Dye-Sensitized Solar Cells. *Chem. Commun.* **2011**, *47*, 2700−2702.
(29) Kawano, R.; Watanabe, M. Equilibrium Potentials and Charge Transport of an I^-/I_3^- Redox Couple in an Ionic Liquid. *Chem. Commun.* **2003**, *3*, 330−331.
(30) Thorsmølle, V. K.; Rothenberger, G.; Topgaard, D.; Brauer, J. C.; Kuang, D.-B.; Zakeeruddin, S. M.; Lindman, B.; Grätzel, M.; Moser, J.-E. Extraordinarily Efficient Conduction in a Redox-Active Ionic Liquid. *ChemPhysChem* **2011**, *12*, 145−149.
(31) Thapa, R.; Park, N. First-Principles Identification of Iodine Exchange Mechanism in Iodide Ionic Liquid. *J. Phys. Chem. Lett.* **2012**, *3*, 3065−3069.
(32) Fei, Z. F.; Kuang, D. B.; Zhao, D. B.; Klein, C.; Ang, W. H.; Zakeeruddin, S. M.; Grätzel, M.; Dyson, P. J. A Supercooled Imidazolium Iodide Ionic Liquid as a Low-Viscosity Electrolyte for Dye-Sensitized Solar Cells. *Inorg. Chem.* **2006**, *45*, 10407−10409.
(33) Guignard, M.; Nazabal, V.; Smektala, F.; Adam, J.-L.; Bohnke, O.; Duverger, C.; Moréac, A.; Zeghlache, H.; Kudlinski, A.; Martinelli, G.; Quiquempois, Y. Chalcogenide Glasses Based on Germanium Disulfide for Second Harmonic Generation. *Adv. Funct. Mater.* **2007**, *17*, 3284−3294.
(34) Wu, W.-Q.; Xu, Y.-F.; Rao, H.-S.; Su, C.-Y.; Kuang, D.-B. Multistack Integration of Three-Dimensional Hyperbranched Anatase Titania Architectures for High-Efficiency Dye-Sensitized Solar Cells. *J. Am. Chem. Soc.* **2014**, *136*, 6437−644.
(35) Wu, W.-Q.; Xu, Y.-F.; Rao, H.-S.; Feng, H.-L.; Su, C.-Y.; Kuang, D.-B. Constructing 3D Branched Nanowire Coated Macroporous Metal Oxide Electrodes with Homogeneous or Heterogeneous Compositions for Efficient Solar Cells. *Angew. Chem., Int. Ed.* **2014**, *53*, 4816−4821.
(36) Wu, W.-Q.; Xu, Y.-F.; Su, C.-Y.; Kuang, D.-B. Ultra-Long Anatase TiO_2 Nanowire Arrays with Multi-Layered Configuration on FTO Glass for High-Efficiency Dye-Sensitized Solar Cells. *Energy Environ. Sci.* **2014**, *7*, 644−649.
(37) O'Regan, B. C.; Durrant, J. R. Calculation of Activation Energies for Transport and Recombination in Mesoporous TiO_2/Dye/Electrolyte Films-Taking into Account Surface Charge Shifts with Temperature. *J. Phys. Chem. B* **2006**, *110*, 8544.
(38) Wang, Z.-S.; Hara, K.; Dan-oh, Y.; Kasada, C.; Shinpo, A.; Suga, S.; Arakawa, H.; Sugihara, H. Photophyscial and (Photo)-electrochemical Properties of a Coumarin Dye. *J. Phys. Chem. B* **2005**, *109*, 3907−3914.